

# Time- and spatially resolved emission spectroscopy of the dielectric barrier discharge for soft ionization sustained by a quasi-sinusoidal high voltage

Vlasta Horvatic<sup>1</sup> · Antje Michels<sup>2</sup> · Norman Ahlmann<sup>2</sup> · Günter Jestel<sup>2</sup> · Damir Veza<sup>3</sup> · Cedomil Vadla<sup>1</sup> · Joachim Franzke<sup>2</sup>

Received: 5 May 2015 / Revised: 3 June 2015 / Accepted: 3 June 2015 / Published online: 16 June 2015  
© Springer-Verlag Berlin Heidelberg 2015

**Abstract** A helium capillary dielectric barrier discharge was investigated by means of time-resolved optical emission spectroscopy with the aim of elucidating the process of the formation of the plasma jet. The helium emission line at 706 nm was utilized to monitor spatial and temporal propagation of the excitation of helium atoms. The discharge was sustained with quasi-sinusoidal high voltage, and the temporal evolution of the helium atomic emission was measured simultaneously with the discharge current. The spatial development of the plasma was investigated along the discharge axis in the whole region, which covers the positions in the capillary between the electrodes as well as the plasma jet outside the capillary. The high voltage electrode was placed 2 mm from the capillary orifice, and the distance between the ground and high voltage electrode was 10 mm. The complete spatiotemporal grid of the development of the helium excitation has shown that during the positive half-period of the applied voltage, two independent plasmas, separated in time, are formed. First, the early plasma that constitutes the plasma jet is formed, while the discharge in the capillary follows subsequently. In the early plasma, the helium atom excitation propagation starts in the vicinity of the high voltage electrode and departs from the capillary towards the ground electrode as well as several millimeters outside of the capillary in the form of the plasma jet. After relatively slow propagation of the early plasma in the

capillary and the jet, the second plasma starts between the electrodes. During the negative voltage period, only the plasma in the capillary between the electrodes occurs.

**Keywords** Dielectric-barrier-discharge ionization · Soft ionization · Time-resolved emission spectroscopy

## Introduction

Since 2007, ionization sources based on dielectric barrier discharges (DBD) intended for soft ionization of molecules have been and are still characterized [1–11]. One of the methods that utilize these sources is the dielectric barrier discharge ionization (DBDI) [12] and is based on a plasma jet established at the end of a capillary dielectric barrier discharge at atmospheric pressure. These discharges producing plasma jets that extend in the surrounding atmosphere are versatile, cheap, and easy to construct devices that have found extensive use as ionization sources in the ambient mass spectrometry techniques. There are various configurations [13] of DBD ionization sources with one or two dielectric barriers, with one or two ring electrodes around the capillary or with an electrode pin inside and one ring electrode around the capillary. Regardless of the configuration, the formed plasma can be separated in two regions: one between the electrodes, henceforth called electrode plasma, and the plasma jet extending beyond the capillary tip into the surrounding atmosphere.

The discharge dynamics in a capillary atmospheric pressure dielectric barrier discharge has been considered in many reports. However, some aspects of the formation of the plasma in the capillary and the jet and their propagation dynamics have not yet been fully understood and remain intriguing. Several theories have been proposed to explain the process

✉ Vlasta Horvatic  
blecic@ifs.hr

<sup>1</sup> Institute of Physics, Bijenicka 46, 10000 Zagreb, Croatia

<sup>2</sup> ISAS—Leibniz Institut für analytische Wissenschaften, Bunsen-Kirchhoff-Str. 11, 44139 Dortmund, Germany

<sup>3</sup> Department of Physics, Faculty of Science, University of Zagreb, Bijenicka 32, 10000 Zagreb, Croatia

of the formation of the so-called plasma bullets that make up the plasma jet.

These plasma bullets have been described using a streamer propagation model based on photo-ionization [14, 15] through computer simulations of streamer propagation [16, 17], with a fast ionization wave discharge [18] and, recently, with the propagation of the plasma diffusion waves [19]. Also, solitary surface waves were considered to be responsible for the formation of the plasma bullets [20], while Jiang et al. [21] reported that the plasma jet is essentially a streamer corona totally independent of, but obscured by, electrode plasma. Additionally, recent experimental observations [22–27] and modeling studies [16, 17, 28] showed that the metastables play a key role in sustaining the plasma bullet propagation along the helium gas channel.

In literature, the most frequently accepted concept of the plasma jet formation and propagation has been based on streamer model, and the plasma jet has been described as streamer-like, guided streamer, cathode directed streamer, anode directed streamer, or streamer corona discharge [21, 23, 26, 29–32]. The strongest argument in favor of considering the plasma jet as streamer-like feature is the order of magnitude of the velocity of its propagation ( $10^3$ – $10^5$  cm/s), which matches the one typical for the streamers. All other plasma jet properties seem to contradict the streamer behavior. Streamers are usually unstable, inhomogeneous, and exhibit random channeling behavior in a wide open space where the discharge path is not restricted. The plasma jets do not share these characteristics since they are stable, reproducible, and spatially well-directed discharges.

In the investigations published so far, the bullets propagation in the plasma jet was predominantly monitored with intensified charge-coupled device (ICCD) camera or photomultiplier, sometimes accompanied with bandpass filters (typical bandpass  $\sim 10$  nm). Therefore, the emission from the jet was measured with poor or no spectral resolution at all.

In the aforementioned investigations, the emission at the particular moment in time was captured from the jet as well as from discharge in the capillary, thus providing complete information regarding the spatial development of the plasma. The time development of the plasma revealed no unusual time correlations between capillary and jet plasma, i.e., the jet was found to be the flow-driven plasma effluent of the capillary DBD.

To our knowledge, there are only two experiments [21, 31] reported in which the discharge current was measured simultaneously with the plasma emission from the jet as well as from the capillary. Both investigations showed that the emission from the jet precedes the discharge in and emission from the capillary, regardless of the different voltage shapes used to drive the DBD (sinusoidal [21] and positive-going unipolar pulse [31]).

The authors [21, 31] concluded that plasma jet and capillary plasma developed in a mutually independent way, and that the jet is not just the discharge swept out from the capillary by the gas flow. The emission measurements [21, 31] were done simultaneously at only two positions, one in the jet and one in the capillary, which were sufficient to identify the occurrence. No attempt was made to further investigate how this interesting phenomenon develops in time and space.

Here, we will present the results of spectrally, spatially, and temporally resolved emission from the plasma that was measured simultaneously with plasma current. Emission of helium 706 nm line is chosen as a representative of excited helium species in the plasma. Investigation of the spatial development of the plasma covers the region between the electrodes as well as the plasma jet. At each investigated position along the plasma axis, time-resolved current and emission signals were measured simultaneously. It will be shown that the plasma jet ignites earlier than the plasma between the electrodes, thus confirming the previous findings [21, 31] that the jet cannot be a subsequent of the electrode plasma or a so-called after-glow. It is a self-contained plasma, which is only coupled to the electrode plasma in a way that the energies coupled into both plasmas are separated. The present results deepen the insight into how these plasmas are formed, by providing a complete spatiotemporal grid of the development of the electrode as well as jet plasma.

## Experiment

The experimental arrangement is shown in Fig. 1. The helium plasma was generated by a dielectric barrier discharge (DBD) burning in a capillary glass tube (outer diameter: 1 mm, inner diameter: 0.5 mm). Two 1-mm-wide electrodes separated by

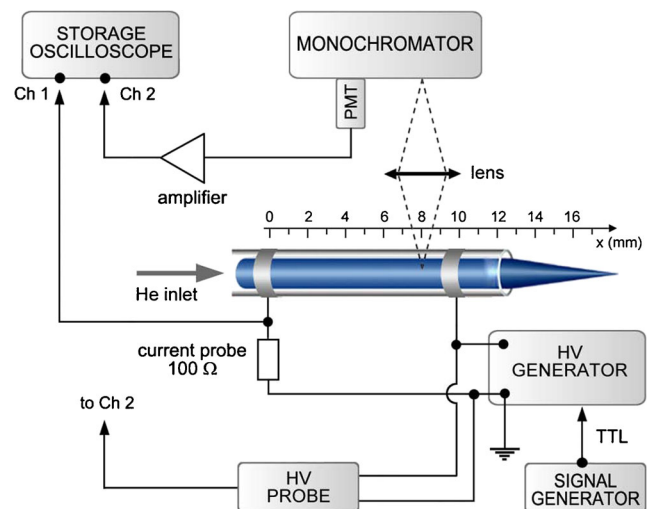


**Fig. 1** The illustration of the experimental arrangement with DBD axial dimension indicated

$\approx 10$  mm surrounded the capillary. The distance from the capillary orifice to the adjacent (front) electrode was approximately 2 mm. The flow rate of helium was kept at  $500 \text{ ml min}^{-1}$ . A micrometer stage, enabling translation of DBD along its axis, was utilized for the spatially resolved measurements along the capillary and the plasma jet.

The voltage applied to the electrodes was supplied by a home built high-voltage generator [33] with maximum peak-to-peak amplitude of 7 kV. A function generator providing rectangular pulses (frequency 21.5 kHz) was used to modulate the high-voltage generator and high-voltage output had a quasi-sinusoidal form.

In all measurements, the voltage amplitude was 3.8 kV and the DBD was working in the homogeneous mode [9]. In contrast to the filamentary mode, which occurs at higher applied voltages, the homogeneous mode is characterized by single positive and negative current peaks during one duty cycle (see Fig. 2a).

The emission from the discharge in the capillary or from the jet was observed at right angles with respect to the discharge axis and imaged with a lens ( $f=10$  cm, imaging ratio: 1:1) onto the entrance slit of a 1-m McPherson monochromator (grating: 1200 grooves/mm) equipped with EMI 9588 QR photomultiplier. The widths of the slits were  $300 \mu\text{m}$ , yielding the band pass of the monochromator of 0.3 nm, and the spatial resolution of 0.3 mm for the used imaging ratio. The spatially resolved helium emission was measured in steps of 0.5 mm, covering the region (see Fig. 1) of the discharge in the capillary ( $0.5 \text{ mm} < x < 8.5 \text{ mm}$ ,  $10.5 \text{ mm} < x < 12.0 \text{ mm}$ ) and in the plasma jet ( $12.0 \text{ mm} < x < 16.5 \text{ mm}$ ).

The photomultiplier current was fed to the home made amplifier (rise time: 0.8 ns), and its output was monitored by 70 MHz digital storage oscilloscope (Agilent DSO-X 2002A).

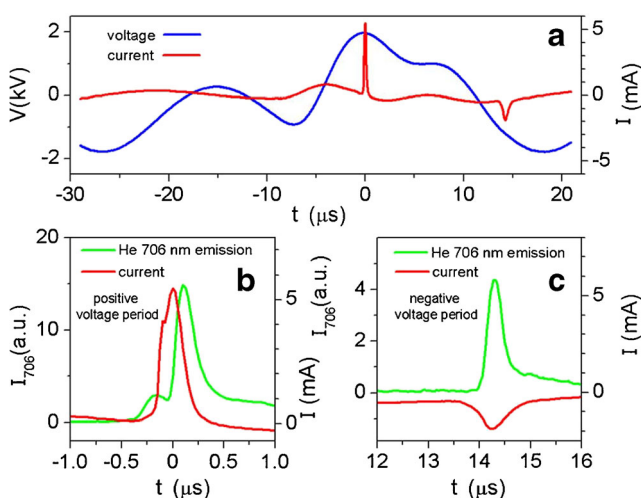


**Fig. 2** **A** Voltage and current signals typical for the conditions in the experiment; **B** current and He 706 nm emission signals in the positive voltage period; **C** current and He 706 nm emission signals in the negative voltage period. The emission signals were measured at position  $x=7$  mm

The voltage signal on DBD electrodes was measured using a high-voltage probe (Tektronix P6015). The discharge current was monitored by measuring the voltage drop over the resistor  $R=100 \Omega$  connected in series with the DBD rear electrode (farthest from the capillary orifice). Both the voltage and the current signals were recorded by the storage oscilloscope.

## Measurements and results

Figure 2a shows the voltage and current signals measured when a generator with quasi-sinusoidal-like voltage shape was used to ignite the DBD.

The current peaks appear subsequent to the steepest voltage change. The positive and negative current peaks occur at the voltages +1.9 and  $-1.2$  kV, respectively. The positive current signal is narrow with higher peak value whereas the negative one is wider and has about three times lower signal height. However, the areas defined by the current signals are comparable, where the area of the positive current is about 40 % higher than for the negative one. The origin of the time scale was set to coincide with the maximum of the positive current peak.

In the course of the present experiment, the time- and space-dependent emission intensities of several helium lines were measured (He 728, He 706, He 587, He 667, He 501, and He 388 nm). All of them exhibited the same intensity distributions in time and space, which are represented here with the results obtained for He 706 nm line.

The current and typical simultaneously measured He 706 nm emission signals in the positive as well as negative voltage period are shown in Fig. 2b, c, respectively. The emission in that figure was measured in the vicinity of the high-voltage electrode inside the capillary at the position  $x=7$  mm. In general, during the positive voltage period (Fig. 2b), He 706 nm emission signal measured along the  $x$ -axis in the capillary exhibits two peaks. The first small peak appears earlier, while the stronger peak is a little bit delayed with respect to the current signal maximum.

During the negative voltage period (Fig. 2c), no double peak structure was observed in the emission signals measured at various  $x$ -positions. Regarding its occurrence with respect to the current maximum, it resembles the stronger emission peak in the positive voltage period.

In the following, the spatiotemporally resolved measurements of the simultaneously recorded discharge current and He 706 nm emission will be presented. The temporal evolution of the He 706 nm signal with respect to the onset of the discharge current maximum was measured in steps of 0.5 mm at series of positions extending from the rear DBD electrode to the plasma jet (see Fig. 1). The results are shown in Fig. 3.

The time scale origin ( $t=0$ ) is set to coincide with the occurrence of the current maximum during the positive voltage

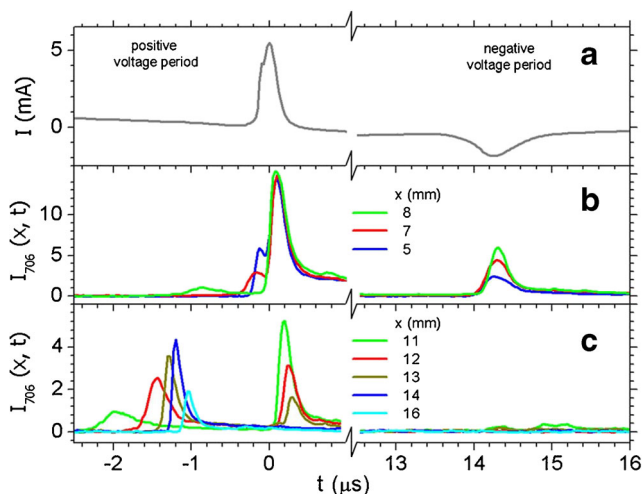


**Fig. 3** Current recorded in positive and negative voltage period (A). Time evolution of the emission intensities of the He 706 nm line measured at several axial positions inside the electrode plasma (B) and along the plasma jet (C)

period (the same as in Fig. 2). The current signals in the positive and negative voltage periods are shown in Fig. 3a. Simultaneously measured emission intensities of the He 706 nm line at several axial positions in the capillary and the jet are displayed in Fig. 3b, c, respectively. Figure 3b displays the time evolution of the He 706 nm emission in the positive and negative voltage period measured along the DBD axis inside the capillary in the region of the electrode plasma. During the positive voltage period, two emission maxima were observed, exhibiting different time separations depending on the point of observation along the axis of the electrode plasma. The stronger signal nearly coincides with the current maximum but is slightly (+80 ns) shifted to a later time. In the following, it will be called coincident peak. The weaker signal, which precedes the coincident signal, will be referred to as early peak. During the negative voltage period, only one signal is detected which has a shift of +80 ns with respect to the current signal. The time evolution of the coincident and early peaks of the He 706 nm emission was also measured at several positions along the plasma jet during the positive and negative voltage period (Fig. 3c).

At this point, it should be emphasized that the transient emission signals were recorded by the oscilloscope working in averaging mode, where the average was made over 32 duty cycles of the high-voltage generator. In the normal, i.e., single recording mode, it becomes apparent that in contrast to the coincident peak, the early peak actually consists of several randomly scattered peaks. This is illustrated in Fig. 4 where three consecutive recordings of the emission signal in the single recording mode are depicted with blue, red, and green lines. The averaging of early peaks over 32 duty cycles of HV yielded a continuous intensity distribution (gray line in Fig. 4), which was used in the data analysis in the present study.

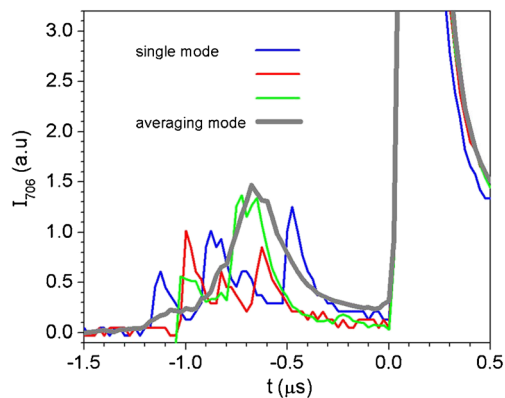


**Fig. 4** Time evolution of the emission intensities of the He 706 nm line measured with the oscilloscope working in single recording and averaging mode. The averaged intensity signal was obtained over 32 duty cycles of the high-voltage generator

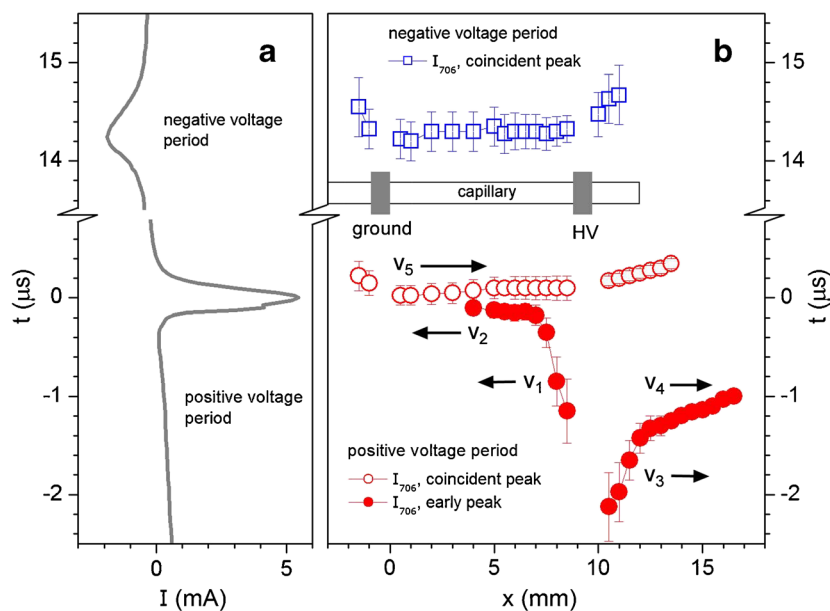
The half-width of each particular early peak in such train of peaks is nearly the same as the half-width of the coincident peak (about 0.15  $\mu\text{s}$ ). On both left and right side in the vicinity of the high-voltage electrode, this scattering is most pronounced and the intensity of each particular early signal is small.

The averaged early peaks in direct vicinity of the high-voltage electrode in the electrode plasma ( $x=8$  mm, Fig. 3b) as well as in the plasma jet ( $x=11$  mm, Fig. 3c) have the broadest half width, the smallest intensity and the biggest time separation with respect to the coincident signal.

The highest measured time separations were measured just next to the high-voltage electrode on both sides at the positions 8 and 11 mm (−1 and 1 mm away from the edge of the HV electrode) and amount to 1.1 and 2.2  $\mu\text{s}$  in the electrode discharge and in the plasma jet, respectively. For larger separations between the HV electrode and the observation position ( $x < 8$  mm,  $x > 11$  mm), the averaged early peak appears closer in time to the coincident peak, and its half width decreases. This is due to the fact that the scattering of the early signal vanishes at larger distances from the HV electrode. The intensity of the early peak measured in the electrode plasma is increasing in the direction towards the ground electrode, i.e., with increasing distance from the HV electrode, and is merging with the coincident signal at positions  $x \leq 5$  mm. However, the intensity of the early peak measured in the plasma jet increases up to position  $x=14$  mm then it decreases. The coincident peaks measured in the plasma jet are delayed by about 200–300 ns with respect to the current maximum, depending on the observation position.

In order to compare the point in time of the maximal emission intensities of the early as well as the coincident peak as a function of the measurement position, Fig. 5 has been prepared. This figure consists of two parts. The left part shows the time evolution of the current. Note that the time scale is ascribed to the ordinate. As in the previous

**Fig. 5** **A** Time evolution of the DBD current. The origin of the time scale ( $t=0$ ) is set to an instant of the current signal maximum in the positive voltage period. **B** Spatiotemporal positions of the He 706 nm peak emission intensities. Red symbols: early (filled dots) and coincident (open dots) peaks in the positive voltage period. Blue symbols: coincident peak in the negative voltage period. The error bars represent the half-widths of the measured transient emission signals



figures, the time scale origin ( $t=0$ ) is set to coincide with the occurrence of the maximum of the current signal during the positive voltage period. Note that the time scale is truncated between 1.2 and 12.8  $\mu\text{s}$  to depict the positive and the negative current period. The right part shows the times at which the maximum emission signals were measured at different positions along the capillary and the jet. The position scale origin  $x=0$  is set on the right edge of the ground electrode. The positions between  $x=0$  and  $x=8.5$  mm refer to the electrode plasma and the positions  $x>10$  mm to the plasma jet. The red full dots depict time points as a function of the position when the emission maxima of the early peaks appear whereas the red open dots and the blue open squares correspond to the coincident peaks measured in the positive and negative voltage period, respectively.

The early emission signals first appeared in the vicinity of the HV electrode, where the earliest of them occurred in the plasma jet at position  $x=10.5$  mm. It appears 2.2  $\mu\text{s}$  before the positive current peak, whereas the first emission signal in the electrode plasma at  $x=8.5$  mm was registered 1.1  $\mu\text{s}$  before the positive current peak.

The velocities of the moving emission front, i.e., the He excitation propagation in particular discharge regions, can be deduced from the  $t-x$  diagram in Fig. 5. In the direction towards the ground electrode starting from  $x=8.5$  mm to  $x=7$  mm, the maximum of the early peak emission signal is moving with a velocity of  $v_1=1.3$  km/s and from  $x=7$  to  $x=4$  with a velocity of  $v_2=40$  km/s. For  $x<4$ , the occurrence time of the early peak coincides with the time of the shoulder of the current peak. In the region from the HV electrode to the capillary orifice ( $x=12$ ), the velocity of the early peak emission signal amounts to  $v_3=2$  km/s, and thereafter, ( $x>12$ ) it proceeds with  $v_4=11$  km/s.

The presented results show that during the positive voltage period in the region between the electrodes as well as in the plasma jet, the emission from the excited helium species was present before the plasma was ignited in the capillary. The helium excitation front starts moving from the high-voltage electrode and propagates to both sides with a speed of about 2 km/s along the first 2 mm and then with a speed higher than 10 km/s along the rest of the path towards the ground electrode and into the plasma jet. It is obvious that in the presented case, the plasma jet was already ignited before the electrode plasma started. Therefore, it can be stated that the propagation of the excitation of He atoms in the plasma jet is not a consequence of the excitation processes in electrode plasma. The plasma jet appears in an earlier phase than the capillary discharge, which coincides with the measured current signal. Simultaneously, with the plasma jet, similar slow propagation of early emission occurs in the capillary in the direction towards the grounded electrode.

When the relatively slowly moving early peak emission in the capillary reached the grounded electrode ( $x=0$ ), the discharge in the capillary ignited, which was accompanied with the coincident emission peak which started to propagate in direction towards the HV electrode, first with a velocity of  $v_5=70$  km/s up to position  $x=4$  mm, and then with an even higher velocity in the region up to the HV electrode. After that, at distances  $10<x<13.5$ , covering the path from the outer HV electrode edge to the capillary orifice and the initial few millimeters of the plasma jet region, the coincident intensity peak propagated with a velocity of 19 km/s. At the positions in the jet larger than  $x=13.5$ , the coincident peak was no more measurable.

In the case of the negative voltage period, no emission outside of capillary was observed. Along the capillary, only

the coincident emission peak was observed, occurring at times that practically overlap with the current signal maximum. Regarding the small time spread of these data (blue open symbols in Fig. 5) and the corresponding error bars, an estimation of the velocity of excitation propagation was not possible.

The intensities of the measured He 706 nm emission peaks are shown in Fig. 6. The red dots symbolize the intensities measured during the positive voltage period (early peak emission: full symbols, coincident peak emission: open symbols). The blue dots depict the emission intensities recorded during the negative voltage period. Starting from the high-voltage electrode, the early peak emission intensities increase with increasing distance towards the grounded electrode as well as in the plasma jet. At distances of about 4 mm on both sides of the HV electrode, a maximum is reached. The coincident signal has a constant emission intensity throughout the capillary. The coincident emission peak intensity is higher than the maximum of the early emission peak intensity directly behind the HV electrode ( $x=10.5$ ) but is rapidly decreasing to the point where the early peak intensity shows a maximum in the jet. It has to be noted that the jet accompanying the coincident signal completely terminates at a distance of only 1.5 mm from the capillary orifice ( $x=12.5$  mm). Compared to that, the jet formed during the early signal is much longer and extends more than 4.5 mm beyond the capillary orifice where the He 706 nm emission peak intensity is still as high as half of its maximum value. Therefore, only the jet formed during the early peak emission can be considered as the one bearing substantial relevance on applications in soft ionization techniques.

The addition of all three signals, which is shown as total intensity with gray line in Fig. 6, gives a measure for the number of excited He\* atoms that is comparable with time-averaged measurements performed earlier [8–10]. The populations of He\* atoms created in higher lying excited states

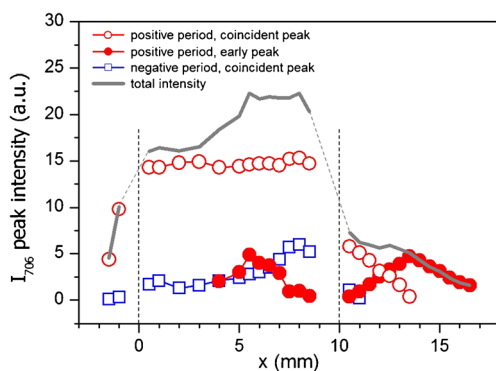


**Fig. 6** Spatial distribution of the He 706 nm emission peak intensities along the electrode plasma and the plasma jet axis. Results are depicted for the coincident peaks measured in the positive and negative voltage periods, as well as for the early peak observed in the positive voltage period. The total intensity comprising all contributions is shown with full line. Vertical dashed lines indicate positions of the outer edges of the electrodes

eventually relax, resulting with the accumulation of the population in the metastable states, which are the lowest excited He states. Therefore, the emission from the higher excited states, e.g.,  $3s^3S$  (706 nm radiation) in the present experiment, can serve as a measure of the helium metastable population. As shown previously [9], in helium capillary DBD working in homogeneous mode, ionized nitrogen molecules  $N_2^+$  are formed by Penning ionization of neutral nitrogen  $N_2$  in collisions with He metastable atoms. The presence of  $N_2^+$  in an ionization source is a precursor for a series of cascade processes, which lead to the creation of the protonated water molecules that are essential for the process of the soft ionization of analytes. The previous investigations [8–10] have shown that the spatial distributions of the He\* and  $N_2^+$  emission line intensity are in correlation. Therefore, based on the present results, which have shown that the appreciable He\* population in the plasma jet exists only during the early peak emission, and their consistency with the previous time-averaged measurements [8–10], it can be assumed that outside the capillary the formation of the  $N_2^+$  is directly dependent on the early peak emission signals measured in the plasma jet.

## Discussion

In the investigated system, helium atoms He\* in the excited states are created in collisions of ground state He atoms with electrons by electron impact. The velocities of electrons capable of exciting helium atoms to the relevant upper states of the optical emission lines are of the order of magnitude of  $10^3$  km/s. For instance, the energy of the lowest lying He excited state (metastable  $2s^3S$  state) is 19.82 eV, which requires electron with the velocity of  $2.5 \times 10^3$  km/s to be excited by electron impact. On the other hand, the velocities of the propagation of the helium atoms excitation measured here are significantly smaller. The results presented in Fig. 5 show that, during the positive voltage period, the earliest appearance of the He\* is in the vicinity of HV electrode. This means that at the beginning of the process, free electrons need to be accelerated all the way up to the HV electrode to gain enough energy to excite He atoms. As the process develops, the electrons become capable of exciting He atoms at distances further away from the HV electrode. This means that they start to experience an overall enhanced electric field. The source of the field enhancement could be sought in the presence of the ionized nitrogen molecules  $N_2^+$ . Namely, as already mentioned, the relaxation of helium atoms in higher excited states eventually leads to population of the lowest lying excited He states, i.e., metastable states. The presence of helium metastables He<sup>m</sup> in the environment rich with nitrogen, such as ambient atmosphere to which the plasma jet protrudes, causes creation of ionized nitrogen molecules  $N_2^+$  through Penning ionization of  $N_2$  in collisions with He<sup>m</sup>. In the working gas, the nitrogen is always

present as an impurity so that the mentioned process takes place in the capillary as well. Therefore, it is plausible that the presence of the excited He atoms will be accompanied with building up the  $N_2^+$  population. Under the influence of the electric field, the ionized nitrogen molecules will move away from the HV electrode and is not unlikely that a cloud of a positive space charge will be formed in front and behind the electrode, resulting in a transient effective electric field which will accelerate electrons further.

During the negative voltage period, no early emission of the He\* atoms was observed in the plasma jet region. With the polarity of the HV electrode being negative, the free electrons will be accelerated away from the HV electrode and will become energetic enough to produce He\* atoms at distances in the jet where the number density of helium is already substantially low, which, in the present case, would result with weak or non-measurable 706 nm radiation. The accompanying  $N_2^+$  ions will be attracted to the HV electrode, causing the weakening of the transient effective electric field, which will in turn make electrons less capable of exciting He atoms by collisions, and the whole process will eventually cease, thus preventing the formation of the plasma jet.

A better insight in the formation of early excitation could be obtained using a well-defined square-wave high-voltage source. These investigations are currently in progress in our laboratory.

## Conclusion

The present experimental investigation of the spatiotemporal behavior of the excitation of helium atoms in the plasma produced in the capillary dielectric barrier discharge showed that two plasmas separated in time were formed: the electrode plasma which coincides with the ignition of the discharge in the capillary and the early plasma which precedes the latter and on the side of the capillary orifice protrudes in the surrounding atmosphere in the form of the plasma jet.

The early helium emission in the plasma jet, which is an essential part of a capillary DBD applied for soft ionization, occurred only during the rise of the high voltage and in the period of time before the discharge in the capillary region between the electrodes is ignited. No early He line emission outside of capillary, i.e., in the plasma jet region, was observed during the period of negative high voltage. The spatiotemporal measurements of the early peak in the electrode plasma and the plasma jet revealed the propagation of the peak He emission, i.e., the He excitation propagation. This propagation is starting in the vicinity of the high-voltage electrode and is departing in both directions, first slowly with the velocity of the order of 1 km/s, and then with the increased velocity of the order of 10 km/s. The determined values of the excitation propagation velocities are in agreement with previous

investigations [19, 21, 29, 31, 34, 35] dealing with the plasma jet formation within the concepts of streamer and plasma bullet propagation.

The quasi-sinusoidal high-voltage applied here was used in our previous works [8–11] dealing with spatially resolved and the time-averaged emission spectroscopy of the capillary DBD. These investigations showed that there is a correlation between the helium line emission and the emission of  $N_2^+$ . The  $N_2^+$  is commonly accepted as crucial for soft ionization, and on the basis of the present results, it can be assumed that its formation in the plasma jet should be attributed to early plasma, which is followed by the electrode plasma. In addition, it is not excluded that the formation of the  $N_2^+$  influences formation of the effective transient electrical fields in this slowly developing early plasma.

**Acknowledgments** The financial support by the Ministerium für Innovation, Wissenschaft und Forschung des Landes Nordrhein-Westfalen, the Bundesministerium für Bildung und Forschung, the Deutsche Forschungsgemeinschaft (project no. FR 1192/13-1) is gratefully acknowledged. This work has been supported in part by the Croatian Science Foundation under the project no. 2753.

## References

1. Chan GCY, Shelley JT, Wiley JS, Engelhard C, Jackson AU, Cooks RG, Hieftje GM (2011) Elucidation of reaction mechanisms responsible for afterglow and reagent-ion formation in the low-temperature plasma probe ambient ionization source. *Anal Chem* 83(X):3675–3686
2. Xiong Q, Lu X, Liu J, Xian Y, Xiong Z, Zou F, Zou C, Gong W, Hu J, Chen K, Pei X, Jiang Z, Pan Y (2009) Temporal and spatial resolved optical emission behaviors of a cold atmospheric pressure plasma jet. *J Appl Phys* 106(X):083302
3. Urabe K, Ito Y, Tachibana K, Ganguly BN (2008) Behavior of  $N_2^+$  Ions in He microplasma jet at atmospheric pressure measured by laser induced fluorescence spectroscopy. *Appl Phys Express* 1(6):066004
4. Sands BL, Huang SK, Speltz JW, Niekamp MA, Schmidt JB, Ganguly BN (2012) Dynamic electric potential redistribution and its influence on the development of a dielectric barrier plasma jet. *Plasma Sources Sci Technol* 21(3):034009
5. Lu X, Laroussi M, Puech V (2012) On atmospheric-pressure non-equilibrium plasma jets and plasma bullets. *Plasma Sources Sci Technol* 21(3):034005
6. Michels A, Tombrink S, Vautz W, Miclea M, Franzke J (2007) Spectroscopic characterization of a microplasma used as ionization source for ion mobility spectrometry. *Spectrochim Acta B* 62(11):1208–1215
7. Olenici-Craciunescu SB, Michels A, Meyer C, Heming R, Tombrink S, Vautz W, Franzke J (2009) Characterization of a capillary dielectric barrier plasma jet for use as a soft ionization source by optical emission and ion mobility spectrometry. *Spectrochim Acta B* 64(11–12):1253–1258
8. Olenici-Craciunescu SB, Müller S, Michels A, Horvatic V, Vadla C, Franzke J (2011) Spatially resolved spectroscopic measurements of a dielectric barrier discharge plasma jet applicable for soft ionization. *Spectrochim Acta B* 66(3–4):268–273

9. Müller S, Krähling T, Veza D, Horvatic V, Vadla C, Franzke J (2013) Operation modes of the helium dielectric barrier discharge for soft ionization. *Spectrochim Acta B* 85:104–111
10. Horvatic V, Müller S, Veza D, Vadla C, Franzke J (2014) Atmospheric helium capillary dielectric barrier discharge for soft ionization: determination of atom number densities in the lowest excited and metastable states. *Anal Chem* 86(1):857–864
11. Horvatic V, Müller S, Veza D, Vadla C, Franzke J (2014) Atmospheric helium capillary dielectric barrier discharge for soft ionization: broadening of spectral lines, gas temperature and electron number density. *J Anal At Spectrom* 29(3):498–505
12. Na N, Zhao MX, Zhang SC, Yang CD, Zhang XR (2007) Development of a dielectric barrier discharge ion source for ambient mass spectrometry. *J Am Soc Mass Spectrom* 18(10):1859–1862
13. Horvatic V, Vadla C, Franzke J (2014) Discussion of fundamental processes in dielectric barrier discharges used for soft ionization. *Spectrochim Acta B* 100:52–61
14. Lu X, Laroussi M (2006) Dynamics of an atmospheric pressure plasma plume generated by submicrosecond voltage pulses. *J Appl Phys* 100(6):063302
15. Laroussi M, Aken T (2007) Arc-free atmospheric pressure cold plasma jets: a review. *Plasma Process Polym* 4(9):777–788
16. Naidis GV (2010) Modelling of streamer propagation in atmospheric-pressure helium plasma jets. *J Phys D Appl Phys* 43(20):402001
17. Naidis GV (2011) Modelling of plasma bullet propagation along a helium jet in ambient air. *J Phys D Appl Phys* 44(21):215203
18. Takashima K, Adamovich I, Xiong Z, Kushner M, Starikovskaia S, Czarnetzki U, Luggenholscher D (2011) Experimental and modeling analysis of fast ionization wave discharge propagation in a rectangular geometry. *Phys Plasmas* 18(8):083505
19. Kim Y, Han G-H, Jin S, Choi E-H, Uhm HS, Cho G (2014) Measurement of optical signals as a plasma propagation in the atmospheric pressure plasma jet columns. *Curr Appl Phys* 14(12):1718–1726
20. Mericam-Bourdet N, Laroussi M, Begum A, Karakas E (2009) Experimental investigations of plasma bullets. *J Phys D Appl Phys* 42(5):055207
21. Jiang N, Ji A, Cao Z (2009) Atmospheric pressure plasma jet: Effect of electrode configuration, discharge behavior, and its formation mechanism. *J Appl Phys* 106(1):013308
22. Karakas E, Koklu M, Laroussi M (2010) Correlation between helium mole fraction and plasma bullet propagation in low temperature plasma jets. *J Phys D Appl Phys* 43(15):155202
23. Urabe K, Morita T, Tachibana K, Ganguly BN (2010) Investigation of discharge mechanisms in helium plasma jet at atmospheric pressure by laser spectroscopic measurements. *J Phys D Appl Phys* 43(9):095201
24. Li Q, Zhu XM, Li JT, Pu YK (2010) Role of metastable atoms in the propagation of atmospheric pressure dielectric barrier discharge jets. *J Appl Phys* 107(4):043304
25. Niemann B, Boke M, Sadeghi N, Winter J (2010) Space resolved density measurements of argon and helium metastable atoms in radio-frequency generated He–Ar micro-plasmas. *Eur Phys J D* 60(3):489–495
26. Sands BL, Leiweke RJ, Ganguly BN (2010) Spatiotemporally resolved Ar ( $1s_5$ ) metastable measurements in a streamer-like He/Ar atmospheric pressure plasma jet. *J Phys D Appl Phys* 43(28):282001
27. Bussiahn R, Kindel E, Lange H, Weltmann KD (2010) Spatially and temporally resolved measurements of argon metastable atoms in the effluent of a cold atmospheric pressure plasma jet. *J Phys D Appl Phys* 43(16):165201
28. Sakiyama Y, Graves DB, Jarrige J, Laroussi M (2010) Finite element analysis of ring-shaped emission profile in plasma bullet. *Appl Phys Lett* 96(4):041501
29. Boeuf J-P, Yang LL, Pitchford LC (2013) Dynamics of a guided streamer (“plasma bullet”) in a helium jet in air at atmospheric pressure. *J Phys D Appl Phys* 46(1):015201
30. Karakas E, Akman MA, Laroussi M (2012) The evolution of atmospheric-pressure low-temperature plasma jets: jet current measurements. *Plasma Sources Sci Technol* 21(3):034016
31. Sands BL, Ganguly BN, Tachibana K (2008) A streamer-like atmospheric pressure plasma jet. *Appl Phys Lett* 92(15):151503
32. Sands BL, Huang SK, Speltz JW, Niekamp MA, Ganguly BN (2013) Role of Penning ionization in the enhancement of streamer channel conductivity and Ar( $1s_5$ ) production in a He-Ar plasma jet. *J Appl Phys* 113(15):153303
33. Heming R, Michels A, Olenici SB, Tombrink S, Franzke J (2009) Electrical generators driving microhollow and dielectric barrier discharges applied for analytical chemistry. *J Anal Bioanal Chem* 395(3):611–618
34. Teschke M, Kedzierski J, Finantu-Dinu EG, Korzec D, Engemann J (2005) High-speed photographs of a dielectric barrier atmospheric pressure plasma jet. *IEEE Trans Plasma Sci* 33(2):310–311
35. Shi JJ, Zhong FC, Zhang J, Liu DW, Kong MG (2008) A hypersonic plasma bullet train traveling in an atmospheric dielectric-barrier discharge jet. *Phys Plasmas* 15(1):013504